Time-Resolved Absorption Difference Spectroscopy of the LH-1 Antenna of *Rhodopseudomonas viridis*

René Monshouwer,* Andrius Baltuška,† Frank van Mourik, and Rienk van Grondelle

Department of Physics and Astronomy, Free University of Amsterdam, de Boelelaan 1081, 1081 HV Amsterdam, The Netherlands

Received: December 3, 1997; In Final Form: February 27, 1998

The LH-1 antenna of the purple bacterium *Rhodopseudomonas viridis* has been investigated using femtosecond pump−probe spectroscopy. We find that qualitatively the relaxation processes are comparable to those in *Rhodobacter sphaeroides* and *Rhodospirillum rubrum*. Both the spectral relaxation and depolarization take place in approximately 150 fs, which suggests that the excitations in the LH-1 ring are delocalized over two to three pigments. Strong oscillations of the pump−probe signal are observed at all temperatures. We conclude that these must be of a vibrational origin and could be related to the observed fine structure seen in the low-temperature absorption spectrum of *Rps. viridis* membranes. The main frequencies of the oscillations are 65 and 105 cm^{-1}, and the damping time is ∼700 fs. From the amplitude of the oscillations and the slow damping time, we conclude that excitations are transferred in a vibrationally coherent manner from site to site.

I. Introduction

The primary events in photosynthesis are the absorption of light, transportation of the associated energy, and conversion into a stable electrochemical potential. The latter task is performed in a highly specialized pigment−protein complex called the reaction center. The first two tasks are performed by so-called light harvesting or antenna complexes (see for a recent review ref 1). In the past years, much progress has been made in the structural knowledge of photosynthetic complexes. In plant systems the structures of the PS I, PS II, and LHC II complexes are known with moderate resolution (3.4−8 Å).[2−4] One of the first reports of antenna and reaction center organization in bacterial photosynthetic membranes was made by Miller et al. of *Rps. viridis*.[5] These membranes have a pseudocrystalline organization of the RC core complexes in vivo, which enables electron microscopy combined with Fourier analysis techniques to picture the membrane with a resolution up to 20 Å.[5,6] These results for the first time demonstrated that the antenna systems in purple bacteria are organized in a regular circular manner, in the case of the LH-1 complex of *Rps. viridis* in a circle around the RC. In 1995 the first high-resolution three-dimensional X-ray structure of a bacterial antenna complex was published by McDermott et al.[7] This revealed that the peripheral (LH-2) antenna of *Rps. acidophila* consists of a circular aggregate of nine dimeric pigment protein units, a dimer consisting of an α and a βpolypeptide, each binding a bacteriochlorophyll molecule at a conserved histidine residue located in the transmembrane helical stretch of the protein.[7,8] The distances between neighboring pigments are approximately 9 Å, suggesting that there is relatively strong electronic coupling between them. For the LH-2 complex of *Rps. molischianum* the high-resolution three-dimensional structure has now also been solved, and this complex is comparable to that of *Rps. acidophila* but consists of eight dimeric units.[9] Karrash et al.[10] have shown that reconstitution of dimeric LH-1 subunits resulted in spontaneous 2D crystallization into a 16-fold symmetric ring, resembling in size very much the electron microscopy results of Miller and Stark et al.[5,6] Due to this accumulating evidence, it is now generally accepted that a circular organization of α,β pigment−protein subunits is a general feature of antenna complexes of purple bacteria.

While the high-resolution structures give the precise spatial organization of the pigments within the antenna complexes, in general, the function of the protein is not only to "fix" the pigments at a specific position and orientation but also to influence the spectral properties through specific and nonspecific pigment−protein interactions. This has for instance been shown by studying the influence of specific point mutations in the protein surrounding the Bchl pigments.[11,12] All high-resolution structures suggest a high degree of symmetry in the antenna complexes. In the LH-2 complex of *Rps. acidophila* for instance, only two different environments for the Bchl molecules can be discerned: the binding sites belonging to the α and β polypeptide. From the X-ray structure it is clear that the β pigment is slightly bent. This shows that, apart from influencing the electronic (π) structure of the pigment, the protein environment can even influence the shape of the pigment,[7] which is known to have a strong influence on the spectroscopic properties of these pigments.[13] Calculations to model the circular dichroism of this complex have given additional indications for a spectral heterogeneity associated with the α and β pigments.[14] The spectral heterogeneity is however not visible in the (low-temperature) absorption spectra of the Bchl *a* containing antenna systems, suggesting that in these systems the splitting is much less than the inhomogeneous and homogeneous broadening. Contrary to the Bchl *a* containing purple bacteria, *Rps. viridis* does show a spectral heterogeneity in the low-temperature absorption spectra. At cryogenic temperatures, four different bands can be discerned in the absorption spectrum.[15] One of the possible explanations for the fine structure is that the above-

* Corresponding author. Fax +31 20 44 47899. Tel +31 20 44 47930. E-mail biomons@nat.vu.nl.

† Present address: Department of Chemical Physics, University of Groningen, Nijenborgh 4, 9747 AG Groningen, The Netherlands.

S1089-5639(98)00412-5 CCC: $15.00
Published on Web 04/22/1998

mentioned $\alpha-\beta$ heterogeneity is much stronger than the other broadening effects in this system. Furthermore, in the membrane preparations, additional asymmetry in the structure can be introduced by the presence of the reaction center in the center of the ring. Since the reaction center is asymmetric, the ringlike structure is distorted and could cause spectral heterogeneity. McGlynn et al. have demonstrated that there are less subunits present per reaction center when the puf-X protein is present during the synthesis of the photosynthetic membrane.[16] From this they conclude that probably, in vivo, the LH-1 ring is not complete but that a section of the ring is occupied by the puf-X protein. This protein is assumed to play a role in the quinone transport to and from the reaction center and is an additional symmetry-breaking factor that could cause spectral heterogeneity. Apart from arguments based on structural heterogeneity, alternate explanations for the observed heterogeneity are exciton interaction[17] or the presence of a strong vibrational structure of the individual chromophores. Note that the latter would imply relatively large Franck−Condon factors for some specific low-frequency vibrations.

One of the main functions of the antenna complex is to transfer excitations through the membrane to the reaction center. Many time-resolved measurements with subpicosecond time resolution have been performed to monitor the rate and mechanism of energy transfer in LH-1 and LH-2 antenna complexes of different species. These have been done using fluorescence up-conversion, pump−probe, and photon echo techniques.[18−32] They have shown that after excitation very fast relaxation takes place (<1 ps) which is most probably due to excitation migration. This relaxation shows up in pump−probe and fluorescence measurements as a spectral red-shift of the absorption difference spectrum and depolarization of the emission, respectively. Both phenomena have been analyzed in terms of excitation migration in inhomogeneously broadened molecular aggregates. Inhomogeneity in bacterial antenna complexes has been extensively studied using methods such as fluorescence line narrowing and hole burning and probably has a width in the range 200−400 cm^{-1} for different complexes.[33,34] Both the dynamic spectral relaxation and depolarization could be understood with these amounts of inhomogeneity. Recent calculations have shown that inhomogeneity has considerable influence on the spectral properties of these circular complexes,[17,20,31,35,36] and needs to be incorporated to explain steady-state and dynamic properties of these complexes. In the core antenna of *Rps. viridis*, due to the possible heterogeneity, the relaxation could be different from the apparently only inhomogeneously broadened LH-1 antenna complexes of *Rb. sphaeroides* and *Rs. rubrum*. Time-resolved measurements with picosecond resolution have shown that relaxation in the antenna is fast and that trapping in *Rps. viridis* takes place with approximately 60 ps at room temperature.[37] The time resolution in these experiments was however not large enough to resolve the fast energy-transfer processes that take place in the antenna. To further investigate the nature of the inhomogeneity and heterogeneity in the core antenna of *Rps. viridis*, we have performed pump−probe measurements at different temperatures on photosynthetic membranes with ∼100 fs time resolution. While the spectral relaxation is qualitatively similar to that found in other systems, there are some distinct differences in *Rps. viridis*. Most notably the coherent oscillations observed in the pump−probe measurements are very pronounced in *Rps. viridis*, even at room temperature. An analysis of the temperature and wavelength dependence of the oscillations suggests that conventional transfer mechanisms cannot explain the slow damping of the modulations but that some form of vibrationally coherent transfer of excitations takes place.

II. Materials and Methods

Samples were prepared as described before.[15] For the low-temperature measurements, the membranes were diluted in a buffer containing ∼70% glycerol and 100 mM potassium buffer (pH 7.8). For the room-temperature measurements the sample was put in a rotating measuring cell (light path 3 mm) and spinned at a frequency of approximately 45 Hz (∼13 m/s). This ensures that (at a repetition rate of 100 kHz) the sample receives at most two pulses before being refreshed. In the low-temperature measurements the sample was put in a 3 mm acrylic cuvette and cooled using a UTREKS helium flow cryostat. A 15 cm lens was used to focus both pump and probe beams in the sample (spot size ∼150 μm diameter), and the typical excitation intensity was 0.02−0.1 nJ/pulse. Probe intensity was typically 10 times lower. Femtosecond pulses at 800 nm were generated using a titanium:sapphire-based oscillator (Coherent, MIRA) and regenerative amplifier (REGA). This combination generates 180 fs, 4 μJ pulses around 800 nm at a repetition rate of 100 kHz. Twenty-five percent of the pulse is used to generate a white light continuum by focusing the beam in a 2 mm thick sapphire disk. Part of the continuum is compressed using a prism compressor and used as the probe pulse. The dispersion of the continuum was corrected in the wavelength region around 1000 nm by measuring the probe wavelength dependence of the optical Kerr signal of a CS_2 sample.[38] The remaining chirp after correction was cubic, with a maximum deviation of less than 40 fs in the range between 960 and 1070 nm. The measured traces were corrected for this after the measurement by artificially shifting the zero point of the measured kinetics. The remaining part of the continuum was used to seed a double-pass optical parametric amplifier (OPA-9400, Coherent). The OPA is pumped with the frequency-doubled remainder of the fundamental 800 nm REGA output. From the output of the OPA, the idler is selected using cutoff filters, and the pulse was compressed by placing 2.5 cm of glass (BK7) in the beam. This way of compressing the pulse was necessary because the idler output of the OPA is negatively chirped. Optimal compression of both idler and white light continuum resulted in a 100−120 fs cross-correlation at 1020 nm (measured using a 0.2 mm BBO crystal at the place of the sample). The pump beam polarization was rotated using a variable waveplate; final cross-extinction of the pump and probe beams was better than 1/200. The detection wavelength was selected after the sample using a $^1/_8$ m monochromator (bandwidth 4 nm), and detection was done using a lock-in technique. The power spectrum was calculated using the S-plus statistical software package (see Results section for more details of the Fourier analysis).

III. Results

Magic Angle Delta Absorption Spectra and Kinetics. In Figure 1 the absorption spectra of membranes of *Rps. viridis* at room temperature and 4 K are shown together with the absorption-difference spectra at different temperatures, 1.6 ps after excitation. The absorption spectra are essentially equal to those presented earlier.[15] Remarkable is the large red-shift and narrowing of the near-infrared absorption band upon lowering the temperature from 290 to 4 K. In ref 15 at least four Gaussian bands were needed to describe the 4 K absorption spectrum. Recent linear dichroism measurements on these samples have shown that the redmost absorption band (around 1045 nm) has a slightly higher LD/A ratio than the bulk of the

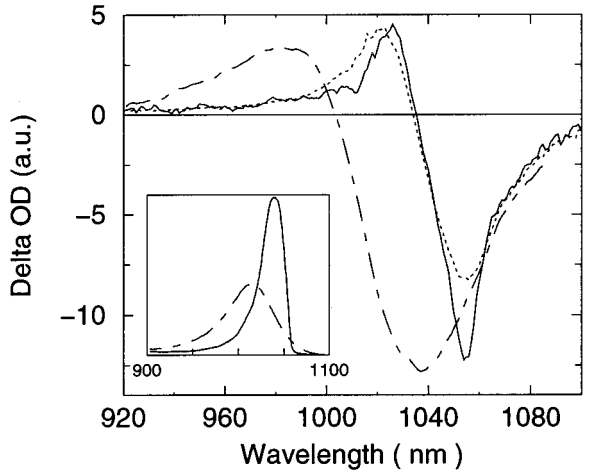

Figure 1. Absorption difference spectra taken 1.6 ps after excitation at room temperature (chain-dash), 77 K (dotted) and 5 K (solid). The spectra were recorded by keeping the delay between pump and probe fixed and scanning the monochromator to spectrally resolve the difference signal. Pump and probe beams were polarized under magic angle. The absolute absorption difference was on the order of 5 mOD; the spectra at different temperatures are not normalized relative to each other. The inset gives the absorption spectrum of membrane fragments of *Rps. viridis* at room temperature (chain-dash) and 4 K (solid).

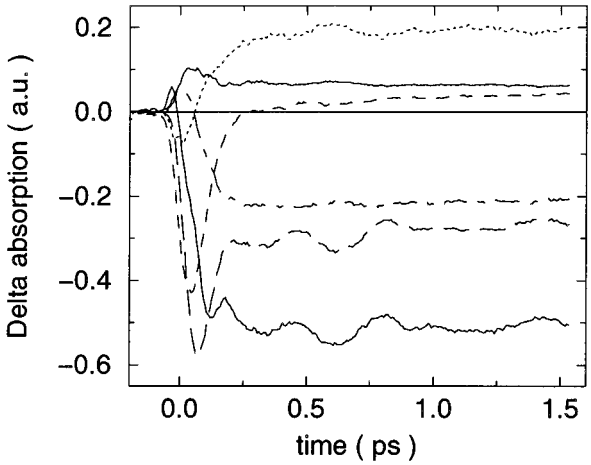

Figure 2. Time-resolved absorption difference measurements upon excitation at 1017 nm and detection at different wavelengths within the Q_y region of the *Rps. viridis* antenna band. The temperature was 77 K. The data shown are part of the data used to construct the absorption difference spectra in Figure 3. Going from top to bottom in the graph, the wavelengths of detection were 1020, 990, 1030, 1070, 1040, and 1050 nm, respectively.

absorption band, thus providing an independent confirmation for the heterogeneous nature of the Q_y absorption band in *Rps. viridis*.[39]

The absorption difference spectra shown in Figure 1 are taken 1.6 ps after excitation. As will be demonstrated below, all major relaxation processes take place within the first picosecond, and thus the spectra after 1.6 ps represent "relaxed" delta OD spectra. Kinetic measurements on a long time scale show that the shape of the delta OD spectrum does not change after ~1 ps but decays in amplitude with a decay time of approximately 150 ps at 30 K.

The shape of the delta OD spectra is qualitatively similar to delta OD spectra observed for other purple bacteria.[18,19,25,27,28,40] The blue part of the spectrum consists of excited-state absorption whereas the red part of the spectrum reflects a sum of ground-state bleaching and stimulated emission. Upon lowering the temperature, the delta absorption spectrum basically follows the changes of the OD spectrum, i.e., the spectrum gets more narrow and shifts to the red. However, especially the 4 K spectrum is differently shaped from the difference spectra obtained at higher temperatures. The excited-state absorption band has become extremely narrow, and the bleaching region appears to consist of a relatively narrow peak superimposed on a relatively broad band.

Figure 2 shows kinetic traces detected at different wavelengths in the Q_y region of the *Rps. viridis* antenna after excitation at 1017 nm at 77 K. After correction, the final uncertainty in the $t = 0$ definition is on the order of 10 fs. First it is clear that most dynamics occur within the first picosecond after excitation. The signals consist of coherent pump−probe and free induction decay contributions around $t = 0$, with superimposed the true population signals. In addition to this, oscillations can clearly be seen in the pump−probe signals lasting up to 1 ps after excitation.

Figure 3a shows a spectral representation of the kinetic data. To generate these time-gated spectra, the signals at each wavelength (spaced 10 nm) were taken at a certain time delay and plotted together as a spectrum. To guide the eye, a smooth curve was generated from the data using a cubic spline interpolation routine and was plotted through the data points.

From the time-gated spectra, we can easily discern three different spectral shapes. The early spectra have a negative signal around 1030 nm, whereas to the red as well as to the blue the signal is positive. Note that the minimum of the initial signal does *not* coincide with the wavelength of the exciting pulse (1017 nm). This signal is present during the pulse and slightly changes shape (compare the −40 and −7 fs spectra in Figure 3a). At later times (125 fs) a spectrum is formed that has a large negative signal around 1040 nm and a positive band peaking at 1005 nm. The final spectrum is slightly broader than the 125 fs spectrum and has shifted to the red (a negative peak at 1055 nm and a positive band at 1020 nm). To do a more thorough analysis of the spectral evolution and to estimate the time scale of the changes, we have performed a global analysis of the kinetic data using a sequential model. We find that a satisfactory fit could be obtained using two sequential states together with a pulse following contribution that accounts for the fast early signals. The time required for the first state to convert into the second state was 150 fs. The corresponding species-associated spectra are shown in Figure 3b. The pulse-following contribution has a shape that strongly resembles the early time spectra shown in Figure 3a. The initially created and final spectrum are comparable to the 125 fs and 1.1 ps spectra of Figure 3a, respectively. The final spectrum is ~10 nm red-shifted with respect to the initially created state. To compare with similar measurements by Visser et al.,[18,19] we have extracted the location of the zero crossing from the interpolated data. We note that the spectral resolution is much lower in our experiment, and the coherent artifact significantly disturbs the initial part of this shift. However, the typical decay (1/e) time of the zero crossing of the interpolated data was 130 fs, which is close to the time constant derived using the spectral fitting model.

Figure 4 shows the spectral evolution of the absorption difference spectrum at 77 K upon excitation at 1036 nm. The shape of the spectra is very comparable to those observed upon excitation at 1017 nm. A clear difference is however that no or hardly any red-shift of the zero crossing is seen in the pump−probe spectrum. The end spectra are equal within experimental error.

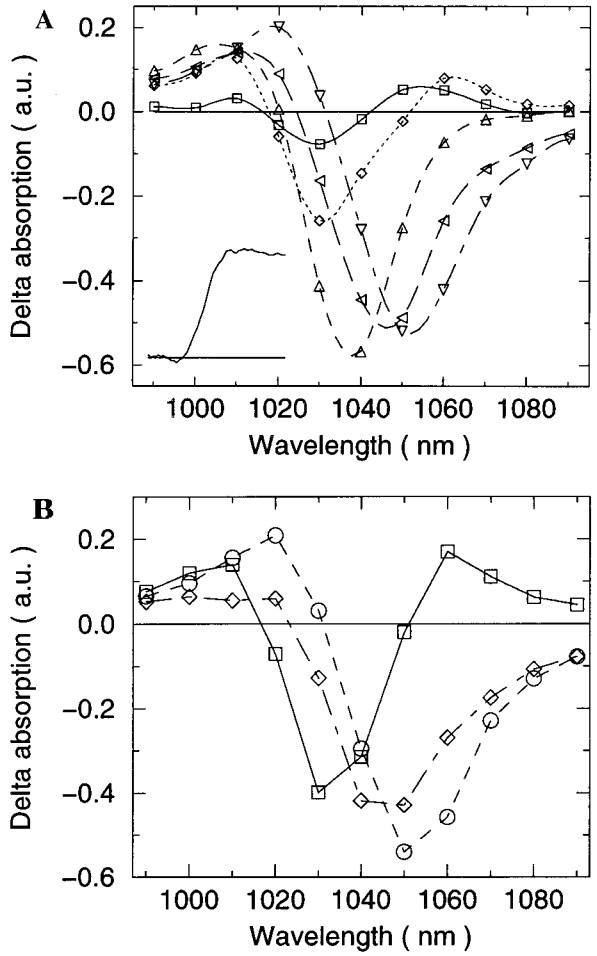

Figure 3. (A, top) spectral representation of kinetic traces obtained upon excitation at 1017 nm at 77 K (see Figure 2). Shown are spectra at time points −40 fs (squares), −7 fs (diamonds), 60 fs (triangles pointing up), 125 fs (triangles pointing left), and 1.1 ps (triangles pointing down). The symbols represent the true data points; the lines are spline fits to the data and were added to guide the eye. The inset shows the integrated total absorption difference intensity around $t = 0$ (total time range shown is 350 fs). (B, bottom) Resulting spectra of a global analysis of all the data of the 1017 nm excitation experiment using a three-step sequential model. The first spectrum (squares) is following the pulse. Initially, the diamonds spectrum is formed which relaxes to the final spectrum (circles) with a time constant of 150 fs.

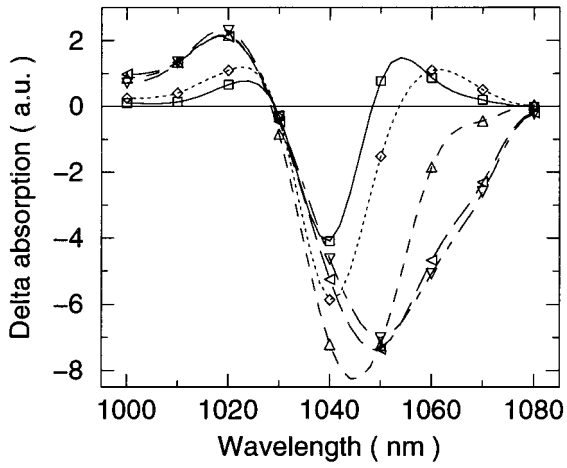

Figure 4. Evolution of the absorption difference spectrum after excitation at 1036 nm. See Figure 3 for details.

Anisotropy. We have measured polarized pump−probe kinetics at a variety of excitation and probe wavelength combinations and temperatures. Figure 5 shows an anisotropy measurement at 4 K upon excitation in the red part of the band (1055 nm). Again, in the region around $t = 0$ strong contributions of coherent coupling are seen in the individual measurements with the probe beam both parallel and perpendicular to the excitation pulse polarization. Shown in the figure is also the anisotropy calculated from both traces and a monoexponential decay function fitted to the anisotropy decay. The decay of the anisotropy takes place with a characteristic time of 150 fs, and the residual anisotropy (after 1.5 ps) is in this case 0.16, which is significantly higher than the value of 0.1 found upon excitation in the middle and the blue part of the band (not shown). Figure 6 shows an anisotropy signal detected at 1050 nm. In this signal clearly oscillations in the calculated anisotropy can be observed. We note that fitting the anisotropy is ambiguous, since the region around $t = 0$ is strongly contaminated with contributions other than from population dynamics. As a consequence, fitting of the anisotropy was started after pump−probe pulse overlap. Furthermore, also the oscillations could contribute to fast phases in the anisotropy signal.

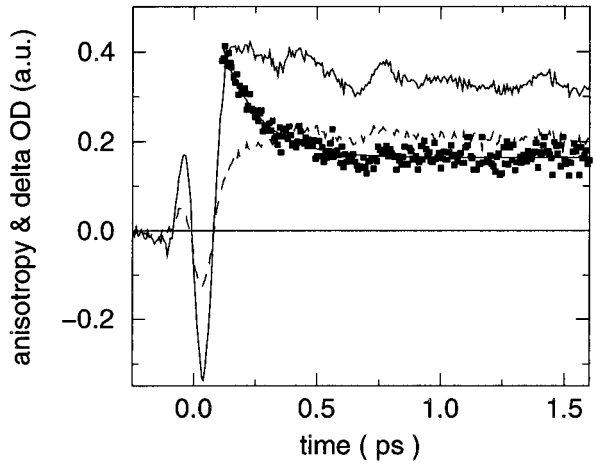

Figure 5. The 5 K anisotropy measurement. Excitation was at 1055 nm and detection at 1070 nm; shown are the parallel (solid), perpendicular (dash) pump−probe response, the calculated (squares) and the fitted anisotropy (solid). The anisotropy was fitted with a 150 fs monoexponential decay and a remaining anisotropy of 0.16.

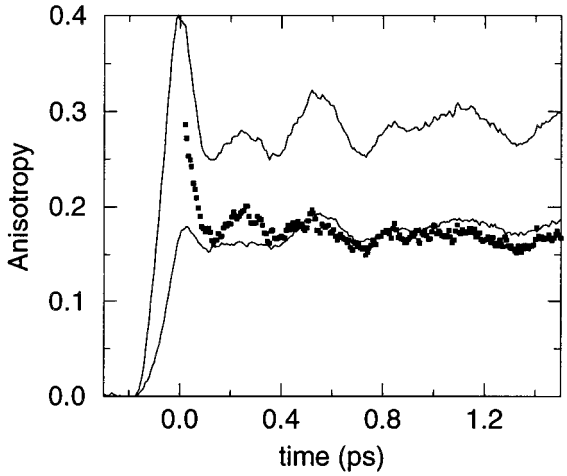

Figure 6. Anisotropy of the pump−probe signal measured after excitation at 1055 nm and detection at 1050 nm. The temperature was 5 K (see Figure 5 for details).

Oscillations. Following the excitation of the *Rps. viridis* LH-1 antenna, strong oscillations are observed at all detection wavelengths and at all temperatures. Even at room temperature

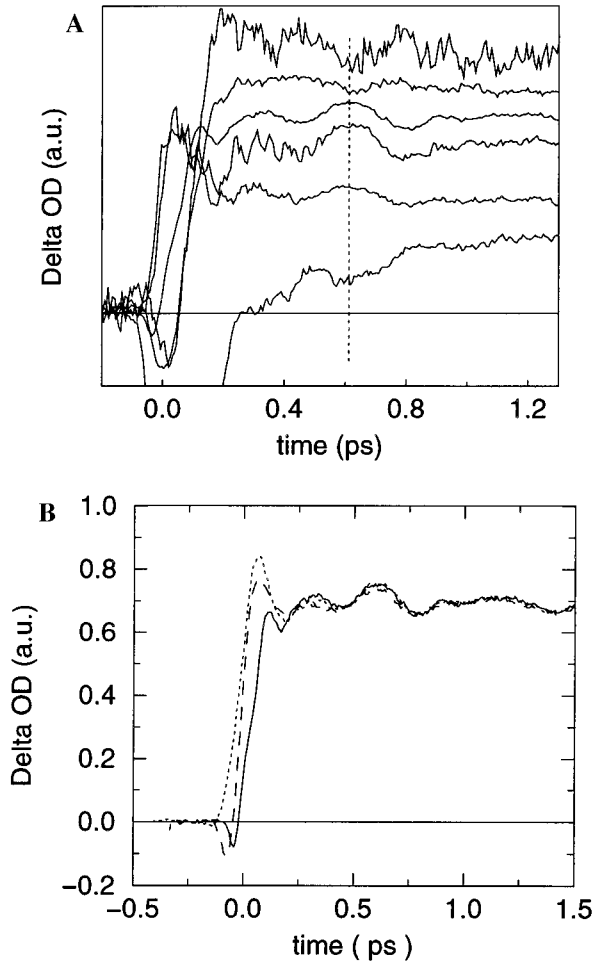

Figure 7. (A, top) Comparison of different traces, focused on the oscillatory patterns. The traces were scaled and some inverted to make comparison easy. From top to bottom, traces at 1090, 1070, 1050, 1010, 990. and 1030 nm are shown. The vertical line was drawn to indicate the approximate maxima and minima in the oscillatory patterns. Excitation was at 1017 nm and temperature was 77 K. (B, bottom) Kinetics after excitation at 1017 (solid), 1036 (dashed), and 1056 nm (dotted). The traces were scaled to make the signal at later times overlap. Detection was at 1050 nm and temperature was 77 K.

(not shown) oscillations with an amplitude of ~20% could be observed. Figure 7a shows traces detected at different positions in the absorption band upon excitation at 1017 nm at 77 K. The dashed vertical line was drawn to indicate the approximate position of the "peaks" or "valleys" in the oscillations of the different traces. It is clear from this comparison that the phase of the oscillation is constant throughout the band, except for a 180° phase flip. A detailed analysis of the data shown in Figures 2 and 3 indicates that there are two points where this phase jump takes place. One is at 1030 nm, slightly blue-shifted from the isosbestic point (which is at 1035 nm at 77 K). The other 180° phase shift takes place between 1060 and 1070 nm. In these traces the maximum relative amplitude of the oscillation was 20% (detection at 1040 nm). Figure 7b illustrates that there is no excitation wavelength dependence of the oscillatory pattern or of the amplitude of the oscillations. The excitation wavelengths in Figure 7b range from ~22 nm to the blue to ~17 nm to the red of the absorption maximum.

Analysis of the Oscillations. Figure 8 shows the residual of the 1040 nm trace from Figure 2 after fitting with a biexponential decay to remove the nonoscillatory part of the signal. To analyze the oscillations, we have fitted the residual with the following function:

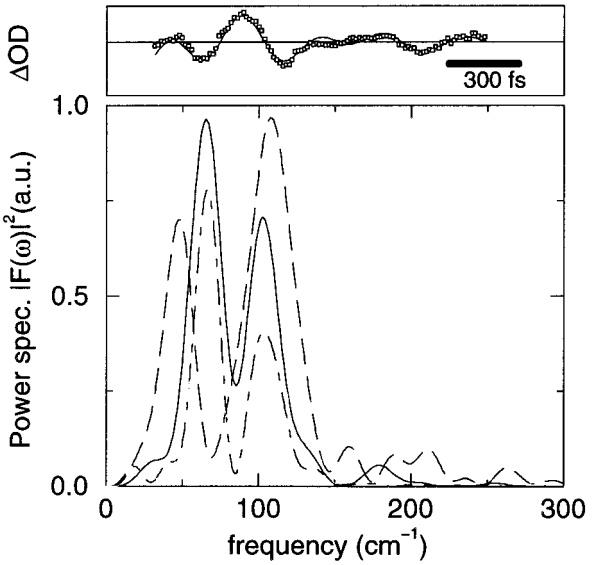

Figure 8. Top part shows the residual of a trace upon excitation at 1017 nm and detection at 1040 nm. The solid curve is a fit to the data using a combination of two decaying sine functions (see text). The parameters of the fit are $\tau_d = 0.78$ps, $\tau_1 = 0.31$ps, $\tau_2 = 0.54$ps, $A_1 = 0.29$, $A_2 = 0.26$, $\phi_1 = 2$, and $\phi_2 = 1.26$. The bottom graph shows the power spectrum of the residuals at different temperatures. Shown are the power spectra at room temperature (dashed), 77 K (solid), and 4 K (dash−dot). The locations and widths of the peaks are given in Table 1.

$$\text{Residual}(t) = \exp\left(-\frac{t}{\tau_d}\right)\left(A_1 \sin\left(\frac{2\pi t}{\tau_1} + \phi_1\right) + A_2 \sin\left(\frac{2\pi t}{\tau_2} + \phi_2\right)\right) \quad (1)$$

The drawn line through the residual in the top of Figure 8 is a fit to the data with this function giving a damping time of 780 fs for both oscillatory components, and frequencies of 61 and 106 cm^{-1} for the oscillations. Given the signal-to-noise ratio of the measurement, no improvement of the fit was observed by adding a separate damping rate for the second mode. A complementary way of analyzing the frequency content of the oscillations is to calculate a power spectrum or periodogram of the residual. To improve the resolution of the power spectrum, the signal was tapered (i.e., zeros were added to the end of the time trace before transformation to increase the spectral resolution of the analysis). In the power spectrum shown in the bottom of Figure 8 two dominant frequencies can be found, at 65 and 103 cm^{-1}. Minor peaks are at 28, 133, and 180 cm^{-1}. The decay time of the modes was derived from the full width at half-maximum (fwhm) of the peaks in the Fourier spectrum using $\tau_d = 1/(2\Delta\nu c)$. The width of the Fourier component (~25 cm^{-1}) corresponds to a decay time of 670 fs, which is close to the damping time found in the nonlinear fitting procedure above. In general, the Fourier spectra of all residuals of the traces between 990 and 1090 nm showed identical features. All Fourier spectra were dominated by two distinct spectral components, one around 65 cm^{-1} and one around 105 cm^{-1}, both with a width of ~25 cm^{-1}. To validate our Fourier analysis method and to determine the systematic errors made in the location and width of the peaks, we have analyzed simulated traces comparable to the measured data (noise and a mono- or biphasic decay was added to two oscillatory components and the data was convoluted with a ~100 fs wide Gaussian pulse representing the instrument response). Errors in the estimated parameters were approximately 10% (location) and 20% (width).

TABLE 1: Locations and Widths of the Two Dominant Modes in the Power Spectrum of the Residual at Different Temperatures[a]

temp (K)	λ_{exc}, λ_{det} (nm)	freq (cm^{-1})	width (τ_d) (cm^{-1} (ps))	freq (cm^{-1})	width (τ_d) (cm^{-1} (ps))
290	1015, 980	48	23.2 (0.72)	108	35.4 (0.47)
160	1017, 1050	65	25.7 (0.65)	103	26.4 (0.63)
77	1017, 1040	65	24.5 (0.68)	103	24.7 (0.67)
4	1055, 1050	67	19.5 (0.85)	104	25.1 (0.66)

[a] Decay times of the oscillations were calculated from the width of the peak in the spectrum using $\tau_d = 1/(2c\Delta)$, where Δ is the full width at half-maximum of the band in the Fourier spectrum. For the analysis a residual was chosen with a large amplitude of the oscillations, general features were however identical for all residuals.

This was also true for "bad" fits (i.e., biphasic fits of monoexponential data, and vice versa). Only low frequency components were strongly dependent on the fit used. This analysis indicates that the estimates of frequency and decay times of the oscillations using the Fourier analysis are reliable for modes above $\sim$40 cm^{-1}. In general, the frequencies found are very comparable to measurements by other groups on Bchl *a* containing antenna systems.[21−23] Two similar modes found have for instance also been observed by Chachisvilis et al. in the LH-1 complex of *Rs. rubrum*[21] (67 and 103 cm^{-1}). Also, the width of the peaks ($\sim$25 cm^{-1}) and thus the damping of the oscillations are very similar to their measurements. We note that the estimates of the kinetics and decay times of the oscillations are based on a model where the observed signal is a sum of exponentially decaying and oscillating terms. In a model where the decay is not exponential but for instance takes place in a coherent fashion (see Discussion), this model does not apply, and the decay rate of the oscillations should be differently analyzed. Fourier spectra of the residuals at other temperatures (5 K, 160 K, and room temperature) showed features essentially identical to the ones described above. In all Fourier spectra the spectrum was dominated by two components around 65 and 105 cm^{-1}, except at room temperature, where the lowest frequency was shifted to 48 cm^{-1}. At typical wavelengths, we have analyzed the Fourier spectrum of the residuals to extract the frequencies of the oscillations, as well as the decay time. The results are shown in Table 1. Most remarkable is that the amplitude of the oscillations is very large, even at higher temperatures. At room temperature oscillations with an amplitude of $\sim$20% (peak to peak) were observed. This weak temperature dependence of the oscillation amplitude is markedly different from the RC and the LH-1 antenna of Bchl *a* containing species, where a strong reduction of the oscillation amplitude was observed when increasing the temperature to 290 K.[21,42] Also note that the decay time of the oscillations is virtually temperature independent.

IV. Discussion

Magic Angle Kinetics. The magic angle dynamics shown in Figures 2−4 are characterized by fast signals during the overlap of the pump and probe pulses, subsequent spectral relaxation and oscillations superimposed on the decay kinetics. Apart from these processes in the first few picoseconds, kinetic measurement on a long time scale indicate that the overall pump−probe signal decays with a time of 150 ps at 30 K. This value found in our measurement is close to the decay of the fluorescence in membranes found by Kleinherenbrink et al.[43] and is due to trapping of excitations by oxidized reaction centers. In our measurements the oxidized state of the reaction center is a consequence of the high repetition rate in combination with the excitation density used. The absolute bleaching of the sample during the measurement was in the order of 5 mOD, equivalent to an excitation density of 1 out of every 200 pigments per pulse. Given the relation between the repetition rate (100 kHz) and the recombination rate of the charge-separated state (6 ms at 4 K), it is evident that the reaction center is permanently in the state $P^+Q_a^-$ during these measurements.

Even though we report experiments at different temperatures, we will, in the analysis, concentrate on the 77 K measurements shown in Figures 2−4. The reason for this is first that the spectral resolution is much higher compared to room temperature and second that the possible amount of permanent hole burning is significantly lower at this temperature compared to 4 K. Hole-burning measurements at 4 K show that significant nonresonant hole burning can take place at this temperature, even upon excitation in the blue part of the band (Monshouwer et al., unpublished results).

The global analysis in Figure 3b demonstrates that a reasonable description of the data shown in Figure 3a can be given using a sequential model with two different spectra and a contribution due to an infinitely fast decay component (pulse follower). The initial (pulse following) signal has a spectral shape roughly equal to the second derivative of the absorption band. This feature is essentially present only during the overlap of the pump and probe pulse and is found for all excitation wavelengths and at all temperatures. Furthermore, we note that in general the minimum of this component is not coinciding with the wavelength of excitation.

Coherent Artifact. It is now well established that in a pump−probe experiment during the overlap of the pump and probe pulse, apart from signals arising from population changes, additional coherent contributions are present in the observed pump−probe signal.[44−46] These contributions arise from the presence of pump polarization during the probe pulse (pump polarization coupling), as well as the so-called "perturbed free induction decay". Cruz et al. have analyzed these contributions and their dependence on the population relaxation time (T_1), the dephasing time (T_2), and the spectral inhomogeneity.[44] Qualitatively, the initial spectra in Figures 3 and 4 agree nicely with the predicted contribution from the free induction decay component in these calculations. The simulations indicate that this contribution has spectral oscillations that decrease in frequency with increasing delay.[44] Very similar features can be clearly seen by comparison of the −40 and −7 fs spectra in Figures 3a and 4. In both measurements, the positive peak of the initial spectra in the red part shifts from around 1055 to 1065 nm going from −40 to −7 fs. This shift is consistent with the signature of the free induction decay described above. Important is however that the amplitude of the oscillations essentially "follows" the pulse. The rate of decay (toward negative time) of the free induction decay is dependent on both the dephasing time and the inhomogeneity. A fast decay is indicative of a fast dephasing and/or a large inhomogeneity. Since the width of the absorption band is determined by these two factors, an important parameter is the ratio between the inverse width of the total absorption band and the pulse length of the excitation and probe pulse. In our experiment, both are approximately equal, which explains the observation that the free induction decay does not extend much before $t = 0$ but essentially coincides with the pulse. We therefore ascribe the first phase in the kinetics to coherent coupling effects and not to ultrafast energy transfer or relaxation. It should be noted that modeling of the spectra with a two-level system is a strong oversimplification. The signal in the blue is mainly due to

excited-state absorption and is thus not properly described in a simple two-level model. This probably explains the strong asymmetry of the coherent features, namely, that the spectral oscillations are much more prominent in the red part of the spectrum than in the excited-state absorption region.

Spectral Relaxation. Several techniques have been used to study the dynamics of energy relaxation in photosynthetic antenna complexes. The (polarized) pump−probe measurements in this paper are most comparable to work done by Visser et al., Chachisvilis et al., Hess et al., Kennis et al., and Nagarajan et al. on the LH-1 and LH-2 complexes of *Rb. sphaeroides*, *Rs. rubrum*, and *Rps. acidophila*.[18,19,21,25,26,28−30,40] Fleming and coworkers have applied both fluorescence up-conversion and three pulse photon echo techniques to investigate the nature and rate of the relaxation.[20,22,31] All techniques consistently demonstrate that, after excitation, a fast (<1 ps) spectral equilibration of the excitation takes place within the antenna complex. The nature of the relaxation is however still a matter of debate, ranging from models considering the exciton to be fully localized on one chromophore (monomer or dimer) to models using complete delocalization of the excitation over the antenna complex. In general, however, the assumption is that the system is excited in a state that is not in thermal equilibrium. Subsequent dynamics represent the evolution of the system toward equilibrium.

Visser et al. monitored the relaxation of the Q_y delta OD spectrum upon nonselective excitation in the Q_x band of the LH-1 complex of both *Rs. rubrum* and *Rb. sphaeroides*.[18,19] Even at room temperature the nonselective excitation does not result in an equilibrium distribution, and relaxation takes place. This is expressed in a shift of the difference spectrum of 12 nm to the red with a main component of 325 fs (*Rs. rubrum*) and 700 fs (*Rb. sphaeroides*) at room temperature. Apart from some small differences, the time-gated spectra in Figure 3 show the same main features as the measurements on these systems. Also, in *Rps. viridis* a ∼10−15 nm red-shift of the zero crossing of the bimodal delta absorption signal is observed. Note however that the excitation was not uniform, as is assumed for the Q_x excitation, but was selective. (The excitation was 22 nm blue-shifted relative to the peak of the absorption band.) Furthermore, the coherent artifact contribution is much smaller in the data by Visser et al., which is due to the Q_x excitation scheme in those experiments. The red-shift of the zero crossing was interpreted by Visser et al. as a thermalization of the excitations by hopping energy transfer between individual dimers on an inhomogeneous lattice. Apart from a shift of the zero crossing, there is also significant dynamic relaxation in the red part of the spectrum. Apart from population transfer, these dynamics are most likely related to dynamics in the excited state of the Bchl molecules (SE) and to coherent artifact contributions. As stated, the Q_x excitation was assumed to result in a uniform distribution of excitations over the inhomogeneously broadened Q_y absorption band. In this work and in recent work by other groups, spectral relaxation in the Q_y region has been monitored in a variety of antenna systems upon direct excitation in the long-wavelength band.[25,26] Comparison of Figures 3 and 4 shows that, as would be expected, the spectral relaxation is dependent on the initial excitation wavelength. Apparently, the initially excited population in the 1036 nm excitation experiment (Figure 4) is much closer to the thermalized "end" population, since the spectral evolution toward this end spectrum is much smaller. This is mainly expressed by the absence of a shift of the zero crossing. Surprisingly, thus the relaxation upon excitation in the Q_x band in *Rb. sphaeroides* and *Rs. rubrum* is most comparable to the "blue" excited data set in *Rps. viridis*. This suggests that either the Q_x excitation does not result in an isotropic distribution or the inhomogeneity is much different in the LH-1 complexes of *Rs. rubrum* and *Rb. sphaeroides* in comparison with *Rps. viridis*. In that respect it is interesting to compare our experiments with those by Kennis et al. and Nagarajan et al. on the LH-2 complex of *Rps. acidophila*.[25,26] Upon excitation in the middle of the B850 band they observe no (<1 nm) red-shift of the spectrum. To further investigate these differences between species, more detailed spectral evolution measurements should be done exciting in both the Q_x and the Q_y region. We note that the strong oscillations seen in the pump−probe signals suggest a relatively strong vibrational progression in this antenna (see below). Since the vibronic bands are broad, excitation via these transitions, which would be the case for the 1017 nm data in Figure 3, results in a uniform excitation of the antenna. This would explain the similarity between the spectral relaxation after Q_x excitation and excitation in the blue part of the absorption spectrum.

Both the spectral model (Figure 3b) and the zero crossing dynamics give a typical time for the relaxation in *Rps. viridis* of ∼150 fs. This is a factor of 2−4 faster than found in *Rb. sphaeroides* and *Rs. rubrum*.[18,19] We note however that there are some differences that might make direct comparison difficult. First the spectral resolution is much lower in our measurement. Second, the instrument response in the experiments of Visser et al. was approximately 4 times longer than in our experiment. Since no deconvolution was done of the data, this could have a pronounced effect on the extrapolated relaxation rate, especially in the case of multiexponential kinetics. We conclude from the magic angle spectra that the spectral relaxation observed in *Rps. viridis* is qualitatively similar to those observed in *Rs. rubrum* and *Rb. sphaeroides* and is dominated by a 150 fs component. Comparison with the simulations by Visser et al. indicates a transfer time between sites (in a hopping model) of less than 100 fs.[18,19] However, the estimate from this simulation is strongly dependent on temperature and spectral parameters such as homogeneous and inhomogeneous broadening of the antenna band. Since these parameters could be very different from for instance *Rs. rubrum*, a direct comparison using these simulations should be treated with caution. Furthermore, the dependence of the spectral relaxation suggests that upon excitation at 1036 nm the initial population is close to the thermalized end population.

Anisotropy. Apart from spectral changes of the isotropic spectra, the electronic relaxation is expressed in a depolarization of the observed signal. Inherently, the pump−probe technique is not the most suitable technique to study this, since the signal is composed of a sum of different components, with (possibly) different signs. This can severely disturb the anisotropy signal. To minimize the contributions of these artifacts, we have looked at the stimulated emission region of the delta absorption signal. Comparison with the OD spectrum shows that at wavelengths above 1060 nm the ground-state bleaching contribution to the difference signal is negligible. Furthermore, we assume that in this wavelength region the excited-state absorption is relatively small. The signal in this region is thus mainly due to stimulated emission and can therefore be directly compared to the spontaneous emission measurements done by Jimenez et al. and Bradforth et al.[20,22] Upon excitation at 1036 as well as 1056 nm, the decay of the emission polarization is essentially monoexponential with a decay time of ∼150 fs. In LH-1 Bradforth et al. found a biphasic decay of the anisotropy with a major 110 fs and a minor 400 fs component.[22] The 150 fs

found in our measurements could be a mixture of these two components which possibly could not be resolved due to a slightly worse S/N ratio in our experiments or due to a different amplitude ratio of these components. The depolarization time is thus quite comparable to that of the LH-1 of *Rb. sphaeroides*. For homogeneous ringlike complexes the relationship between the hopping time and the depolarization time is given by[22]

$$\frac{\tau_{\text{depol}}}{\tau_{\text{hop}}} = \frac{1}{4 \sin^2(360/N)} \qquad (2)$$

A relatively simple lower limit for the hopping time can be derived by estimating the maximum homogeneous line width from the steady-state absorption spectrum. A detailed spectral analysis of the absorption spectrum showed that, at 4 K, the absorption band consists of several bands.[15] The width of these bands was less than 20 nm (190 cm^{-1}) fwhm. If we assume that this width is completely due to lifetime broadening, we can associate a single site lifetime of 90 fs with this spectral width. Since in these antenna systems also back-transfer is possible from neighboring pigments, the decay of the population of a single site is highly multiexponential. However, simulations have shown that on these kinds of circular structures the average single site lifetime is approximately half of the hopping time,[47] which results in a minimum hopping time of approximately 180 fs. Combining the measured depolarization time (150 fs) with the minimum hopping time using eq 2, we find that the effective size of the ring "*N*" is less than 11. From electron microscopy on membranes of *Rsp. viridis*,[5,6] 2D crystallography work of Karrash et al.,[10] and a variety of estimates based on biochemical and spectroscopic methods,[48] it is estimated that the number of pigments in the LH-1 ring is between 24 and 32. Using these numbers for the physical size of the ring, the depolarization rate thus indicates that the "effective" size of an excitation is between two and three pigments. Similar conclusions have been drawn by several groups. Measurements of the radiative rate of different complexes indicated that the exciton is delocalized over several pigments but that this number is much smaller than the total number of pigments in the complex.[35] Similarly, pump−probe measurements by Kennis et al. indicate a moderate delocalization in the LH-2 complex of *Rps. acidophila*.[27] Chachisvilis et al. found that the hopping time that was deduced from the isotropic signals combined with the depolarization found in a pump−probe measurement yields a value for *N* that is much lower than what would be expected for the LH-2 antenna using a monomer (18) as well as a dimer model (9). From this discrepancy they conclude that the excitation in *Rb. sphaeroides* is delocalized over at least four pigments.[28]

The anisotropy measurements probed in the middle of the band exhibit very different behavior. Figure 6 shows an anisotropy signal measured in the bleaching region of the difference spectrum. First the initial decay is much faster. This makes it hard to estimate the decay time since the coherent artifact is also contributing to these early pump−probe signals. Furthermore, the anisotropy shows clear oscillations. No such oscillations of the anisotropy have been observed in the spontaneous emission of other complexes[20,22] or in our measurements on *Rps. viridis* in the stimulated emission region. A natural explanation for this surprising observation is that this measurement is nearly a one-color experiment. Therefore, part of the observed signal is due to nontransferred population ($r = 0.4$) and part due to excitations that are depolarized ($r \sim 0.1$). The final anisotropy signal is a weighed average of these, so $r = (0.4a + 0.1)/(a + 1)$, where a is the ratio of both contributions. It is clear that in this case modulations of the anisotropy can be ascribed to changes in the relative intensity of both contributions at the detection wavelength. This is most likely caused by the specific wavelength dependence of the oscillations. In the measurement shown in Figure 6 this effect is enhanced since it is a one-color experiment, and furthermore, at this wavelength and temperature, there is a relatively large part of nontransferring excitations (see below).

Previous steady-state fluorescence anisotropy measurements have shown that, upon excitation in the red part of the absorption band, the emission is highly polarized.[15] This suggests that no or very little transfer of excitations takes place upon excitation of the low-energy transitions in the broad absorption band; *i.e., the state that is excited is also the state that emits*. Similar high fluorescence emission anisotropy has been observed for various different antenna systems in steady-state[33,49] and time-resolved absorption difference measurements.[40] Our measurements clearly show that, upon excitation in the red part of the band, the residual emission anisotropy is higher than 0.1, the value expected for complete depolarization in a plane. Indeed, as would be expected from the steady-state fluorescence measurements, the pump−probe signal only has a higher "end" anisotropy upon excitation in the very red part of the band (>1050 nm). Moreover, inherent to the short duration of the excitation pulse (∼100 fs) the excitation is relatively broad banded (∼20 nm). Therefore, a considerable part of the excited states will be outside the narrow band corresponding to high polarization,[15] and therefore the overall anisotropy upon femtosecond excitation is limited to significantly lower values than the maximum of $r = 0.4$. The "trapping" of excitations on the lowest state is expected to be temperature dependent, since at higher temperatures the thermal energy is enough to escape from the lowest state to slightly higher lying states. This was confirmed by measuring the anisotropy under the same conditions as in Figure 5, but at 77 K (not shown). The final anisotropy (at 1.6 ps) in this measurement dropped from 0.16 to 0.13, in agreement with the proposed model.

Exciton Model. A number of groups describe the antenna system of photosynthetic purple bacteria as a strongly coupled exciton system.[17,25,50] In this case the spectral relaxation is ascribed to scattering to lower exciton levels. For a completely delocalized exciton model the exciton spectrum consists mainly of transitions from the ground state to the two degenerate next to lowest exciton states. The initial anisotropy of such a system would be 0.7, decaying rapidly to 0.1 due to dephasing between the two degenerate perpendicular exciton states.[51]

Recently, pump−probe measurements with ∼35 fs time resolution were reported for the LH-2 complex of *Rps. acidophila* by Nagarajan et al.[25] They find a decrease of the total delta absorption signal of approximately 30% with a biphasic decay of 33 and 200 fs. Furthermore, the initial anisotropy is much higher than the expected maximum of 0.4. Both effects are described in terms of exciton relaxation of a strongly coupled ringlike structure (full exciton delocalization over the ring). The decay of the total intensity of the signal is ascribed to the relaxation of the excitation to the lowest exciton level. Since this level is dipole-forbidden in a fully delocalized exciton model, this relaxation should be accompanied by the observed decrease of the total signal, as observed by these authors. The measurements on *Rps. viridis* in this paper show a very different behavior. Integration of the spectra in Figure 3a from 990 to 1090 nm reveals no fast components corresponding to a decay or rise of the total area of the pump−probe difference spectrum (see inset). We note however that the time resolution of our measurement is lower than that of Nagarajan et al. A kinetic

phase of 35 fs would have a ~7 times smaller amplitude due to the lower time resolution in our experiment and, if present, might therefore be difficult to observe. The mechanism as described by Nagarajan et al. predicts however a significantly larger amplitude for the fast phase in our 77 K measurements compared to room temperature. At 77 K the thermal energy (k_bT) is 53 cm^{-1}, whereas the gap between the lowest exciton level and the dipole-allowed $k \pm 1$ states in a fully delocalized model is (using reasonable assumptions) larger than 100 cm^{-1}. As a consequence, the final occupation of the lowest exciton state should be larger than 77% (including the degeneracy of the $k \pm 1$ states). A comparison of the absorption difference signal after relaxation (see Figure 1) with the steady-state fluorescence spectrum in ref 15 shows that at least 30% of the signal is due to stimulated emission, and thus is not in the dipole-forbidden $k = 0$ state. Furthermore, recent calculations of the influence of inhomogeneity on the exciton states has shown that already a small amount of disorder causes the lowest state to become allowed.[35] We therefore suggest that the fast decay of the overall signal as observed by Nagarajan et al. is not due to trapping of excitations in the forbidden lowest state but is due to some other process. Possibly the 33 fs component observed in their experiment is partly due to a coherent four-wave mixing effect as discussed above. Kühn et al. have recently calculated energy transfer in LH-2 in the presence of disorder and homogeneous broadening using multilevel Redfield theory.[52] In their simulations they find a dynamic decrease of the total bleaching signal that is qualitatively comparable to the measurements by Nagarajan et al. The rate found in the simulations is however much slower than found in the LH-2 complex of *Rps. acidophila* and should furthermore be easily resolvable in our measurements on *Rps. viridis*. Also, this slow relaxation is not observed in *Rps. viridis*. Even at room temperature the decrease of the total area of the absorption difference spectrum is less than 5% (not shown).

Apart from being related to steady-state and relaxation mechanisms, the tentative exciton interaction could explain the observed oscillations in the pump−probe signals. These would then not be ascribed to a vibronic origin but to beating between different exciton levels that have been simultaneously excited by the broad excitation pulse. In this case one would expect that the spectral relaxation and the decay of the oscillations occur on the same time scale. Our measurements, and measurements on different Bchl *a* containing complexes, have however shown that the decay of the oscillations is a factor of 2−4 slower than the spectral relaxation. Furthermore, in case of quantum beats between different exciton levels, the oscillation frequency should be strongly dependent on the exciton band structure and thus implicitly on the strength of the coupling between the pigments. Kühn et al. have for instance modeled the influence of excitonic interaction within a Chl *a*−Chl *b* dimer on the observed coherent oscillations.[53] They show that the beating frequency is mainly determined by the coupling strength between the pigments. In many different antenna systems in many different species, identical frequency modes have however been found. Since it is very unlikely that the amount of electronic coupling is constant from system to system and furthermore more or less temperature independent, electronic coherence is probably not the cause of the observed oscillations. From the above we conclude that the experimental observations largely exclude an excitonic origin for the oscillations in the pump−probe signal. We note that it is remarkable that no observable influence of the excitonic coupling on the vibronic frequencies is seen since also the vibrational transitions have (dipolar) exciton interaction with neighboring pigments. Even if the dipole moment of the ground state to first vibronic state is a small fraction of the 0−0 dipole strength, one would expect observable changes in the transition frequencies due to exciton interaction between these transitions.

Oscillations. Oscillations as shown in Figures 7 and 8 have been observed in different antenna and reaction center preparations in the past. Vos et al. have measured these oscillatory features in the reaction centers of *Rb. sphaeroides* and *Rb. capsulatus*.[41,42,54] They find oscillatory features with distinct frequencies ranging from 15 to 200 cm^{-1} with damping times of approximately 2 ps at room temperature. In different (bacterial) antenna systems, comparable features have been seen. Also in these systems oscillations in the pump−probe signals as well as spontaneous emission are underdamped and last for approximately 1 ps.[21−23] In the LH-1 complex of *Rb. sphaeroides* the temperature dependence of the oscillations was found to be very strong.[21] In these systems at room temperature hardly any amplitude of the oscillation can be seen, in contrast to *Rps. viridis* for which at some wavelengths oscillations with an amplitude of ~20% are observed at this temperature. Also in the bacterial reaction center there is a very strong temperature dependence of the amplitude of the oscillations,[42] leading to a strong reduction of the amplitude at room temperature.

Nature of the Oscillation. The observed oscillations are generally ascribed to a simultaneous excitation of different excited-state vibrational levels of the molecule due to the broad spectral width of the excitation pulse. This excitation prepares the molecule in a wave function that is a superposition of the different vibronic wave functions, so

$$\Psi(t) = c(0)e^{i\omega t}|e,0\rangle + c(1)e^{i(\omega+\omega_{vib})t}|e,1\rangle + ... + c(n)e^{i(\omega+n\omega_{vib})t}|e,n\rangle \quad (3)$$

In principle, in a four-wave mixing experiment as pump−probe, also a wave packet can be created in the ground state by resonant impulsive Raman excitation. The motion of this wave packet would however not be visible in the excited-state absorption (ESA) part of the delta OD spectrum. Since in *Rps. viridis* the oscillations in the ESA part of the spectrum are virtually identical to the features in the bleaching/stimulated emission part, the contribution of the ground-state wave packet is probably negligible. A similar conclusion was drawn by Bradforth et al. on the basis of spontaneous emission experiments[22] and by Chachisvilis et al. following an analysis of the wavelength dependence of the oscillations.[23] The values of the constants $c(n)$ in eq 3 are determined by both the Franck−Condon factor of the nth vibronic level as well as the intensity of the excitation pulse at the frequency $\omega + n\omega_{vib}$. Also, the vibrational ground-state level in which the molecule was before excitation is important. Certainly at room temperature ($k_bT \sim 200$ cm^{-1}) there is significant population of higher vibrational levels in the ground state. For simplicity, we assume however that the molecule is in the ground-state vibrational level. This is clearly true for the 4 K measurement and partly true for the 77 K experiment (population of the 65 cm^{-1}, $\nu = 1$ level is in that case 23%). Note however that there is very little temperature dependence of the oscillations (see Table 1). In the work presented here, the width of the excitation pulse used is 200 cm^{-1}. Due to this relatively narrow spectrum at most the first and second vibronic level of the 103 and 65 cm^{-1} levels can be excited by the excitation pulse. Furthermore, the Franck−Condon factor is strongly dependent on the vibrational quantum number and is given by[55]

$$\mathrm{FC} = |\langle n_e|0_g\rangle|^2 = (S^n/n!)e^{-S} \quad (4)$$

Note that the *S* stands for the linear electron−nuclear coupling of a *single* vibrational mode. This should not be confused with the total integrated electron−phonon and vibration coupling. Values for *S* were determined by Cherepy et al. for the accessory bacteriochlorophyll of the reaction center of *Rb. sphaeroides*.[56] The values for the vibrational modes below ∼300 cm^{-1} were in the range 0.013−0.036. If we take the upper limit of this range (0.036), we can calculate using eq 4 that the Franck−Condon factors of the first three components of the wave function scale as FC(0):FC(1):FC(2) = 0.96:0.034:0.0006. From this we conclude that, using these values for *S*, only the lowest vibrational level can be excited. Moreover we note that only for $S > 0.2$ the magnitude of the second Franck−Condon factor becomes considerable (>10% of FC(1)).

As described by Vos et al., the dependence of the oscillations on the wavelength of detection is caused by the fact that at different wavelengths different positions of the vibrational coordinate are probed. In the case of a *narrow*, moving wave packet on the excited-state surface, this results in a gradually changing phase of the oscillation over the band. This was indeed observed in the reaction center of *Rb. sphaeroides*.[41] If however, as stated above, only the two lowest vibrational states participate, the wave packet consists of the beating of only the 0th and 1st vibrational wave function. The wave functions of these states are well-known, and the final time-dependent overlap of the wave function with the ground state does not show any wavelength-dependent phase shift. This is in agreement with the measurements shown in Figure 7, which suggests that in *Rps. viridis* mainly the lowest vibrational states are contributing to the observed oscillations. Chachisvilis et al. found in the LH-1 complex of *Rb. sphaeroides* and *Rsp. rubrum* that the phase was a gradually changing function of the detection wavelength, with extremes on the edges of the delta absorption spectra.[23] This would suggest that in their experiment more than just the two lowest vibrational levels were excited, implying that the coupling of the relevant modes to the electronic transition would be much stronger in these systems. There are however no additional indications for larger *S* values of vibrations in these systems. We note that the spectral width of the excitation pulse in their experiments was about a factor 2 larger, which might have been responsible for relatively larger population of the higher vibronic levels.

In the bleaching/stimulated emission region the oscillatory features are in line with those observed in other reaction center and antenna preparations.[23,42] At 77 K, no observable oscillatory features are observed upon probing at 1065 nm. At the same wavelength a π-phase jump of the oscillations takes place. However, in contrast to the reaction center this point does not coincide with the emission maximum[15] but is approximately 10 nm red-shifted.

Amplitude of the Oscillation. In the vibronic model the spectroscopically observed beating is caused by the cross terms when calculating the expectation value of an observable using the wave function in eq 3. The finally observed amplitude is dependent on both the specific expectation value calculated (so among others on λ_{det}) and the values $c(n)$ in eq 3. Of additional influence is the method of analysis used (see Materials and Methods section). In *Rps. viridis*, the Fourier spectrum of the oscillating features consists of two well-separated, narrow modes. This effectively enhances the visibility of the oscillations since congested regions of modes interfere strongly and effectively cause a fast initial decay. The latter is strongly suppressed in our analysis because exponential components are subtracted from the residual. The well-defined Fourier spectra in *Rps. viridis* could be related to a "better defined" or less inhomogeneous structure of this system. This relative enhancement could also explain the apparent contradiction between the wavelength independence of the phase of the oscillations and their relatively large amplitude.

In that sense it is interesting to relate the measured oscillations to the fine structure seen in the absorption band of *Rps. viridis*.[15] In the decomposition of the spectrum, we have found a splitting of 102 cm^{-1} between the lowest energy band and the second band. If we ascribe the spectral heterogeneity to a vibronic progression, there is a remarkable correspondence between the splitting of the bands and the 104 cm^{-1} mode observed in the oscillations. However, in the absorption analysis, no 65 cm^{-1} mode was obtained, and furthermore a description with Gaussian bands is more of a descriptive nature and does not relate to a physical model for the line shapes. To make a more accurate analysis of the possible vibronic nature of the absorption bands and to estimate the Huang−Rhys factors and mode frequencies, we are planning to do spectral line-shape calculations analogous to those by Pullerits et al.[57] using both the temperature-dependent absorption and emission spectra.[39] From Figure 7b it is clear that there is no excitation wavelength dependence of the amplitude of the oscillations. This observation is hard to reconcile with a simple model where the absorption band of *Rps. viridis* consists of a relatively narrow distribution of zero phonon transitions in the red and a vibronic progression extending to the blue of the absorption spectrum. Assuming that the coherent nuclear motion is created upon excitation, one would in this case expect a very large difference in the oscillation (amplitude) between the 1017 nm excitation case (mainly overlap of the pulse with the vibronic lines) and the 1056 nm kinetics (mainly overlap with the zero phonon lines). The different excitation wavelengths should have caused a very a different ratio between the $c(0)$ and $c(1)$ constants and consequently a different beating amplitude.

The time-resolved vibrational coherence as measured in a pump−probe experiment is strongly related to the spectral information of the vibrational structure as determined by steady-state spectroscopic techniques. There is for instance a strong correspondence between the modes observed in the resonance Raman spectra and the oscillations seen in pump−probe measurements. Lutz et al. found Raman bands at 65, 86, 108, 138, 172, and 189 cm^{-1} in the LH-1 complex of *Rb. sphaeroides*.[58] Some of these lines correspond nicely to the main modes found by Chachisvilis et al. in the same system (at 90, 110, and 175 cm^{-1}).[21] The modes reported here seem to correspond to some of these modes, although different lines are prominent in this antenna system. In *Rps. viridis*, the 65 cm^{-1} mode, which was not observed in the time-resolved data of the *Rb. sphaeroides* antenna, is very strong whereas the 90 cm^{-1} mode is absent in our measurements. The observed modes are slightly different from those obtained in fluorescence line narrowing measurements of the LH-1 antenna of *Rps. viridis* (Robert, B. personal communication). The corresponding modes, at 88 and 114 cm^{-1}, are both slightly higher than those found in the pump−probe measurements in this paper. We note that the 88 cm^{-1} mode was measured on the edge of the detection range of the fluorescence apparatus, and the precise frequency of this mode might therefore be slightly distorted.

Decay of the Oscillations. One of the most puzzling aspects is the relatively slow damping of the vibrational oscillations. Especially in an antenna system where rapid energy transfer

takes place, a mechanism of transfer of vibrational coherence should be active to explain a damping time that is much larger than the estimated hopping time. For instance, if we take τ_{hop} = 100 fs, approximately six transfer steps take place before the oscillation coherence is destroyed.

There are several different possible decay mechanisms for the vibrational oscillations. The total width (decay time) of the observed vibrational mode can be divided into a homogeneous and an inhomogeneous contribution. The inhomogeneous contribution represents the spread of the energy spacing between the vibrational levels. This results in a decay of the oscillations due to a free induction decay like process. The homogeneous contribution consists of thermal dephasing and relaxation processes of the vibrational levels. Relaxation processes can occur between the different vibrational levels of the pigment or can be due to electronic transfer to other pigments (population transfer). An estimate of the rate at which these relaxation processes take place can be extracted from the resonance Raman measurements. Note that these give an upper limit to the decay time since in the ground state no population transfer path is present. Even though the Raman measurements probe the ground-state vibrational levels, probably the dephasing and relaxation mechanisms are identical to those in the excited state. Measurements on the accessory chlorophyll in the reaction center of *Rb. sphaeroides* were done by Cherepy et al. using the SERDS technique.[56] The Raman lines found have a width of approximately 20 cm^{-1}, very close to the widths found in the Fourier transform of our residuals. Consequently, we propose that a large part of the ~700 fs decay of the coherent nuclear motion must be due to inherent properties of the pigment and not due to excitation transfer. If we assume that the line width found in the Raman measurements is mainly due to homogeneity, we can calculate that the extra broadening due to excitation transfer is in the order of 10 cm^{-1}, which corresponds to 1.6 ps. To explain that, during the electronic transfer steps there is a very slow decay of the oscillation amplitude, a form of transfer of the vibrational coherence should take place.

Transfer of Vibrational Coherence. Jean et al. have performed model calculations on the transfer of coherence during a charge-transfer process.[59−61] This was modeled by calculating the evolution of a system that consists of a single ground-state potential and two excited-state potentials where tunneling was possible. These simulations have shown that under reasonable circumstances the coherence is effectively transferred from donor to acceptor. However, in this modeling, a single reaction coordinate was used. This is only valid in the strong coupling case, whereas for energy transfer between the pigments in the light-harvesting antenna probably the intermediate coupling case is more valid.

One mechanism for transfer of vibrational coherence to consider is that, just like excitation with a short pulse creates a narrow wave packet on the excited potential, also an impulsive energy-transfer step prepares the acceptor molecule in a narrow wave packet in the Franck−Condon region. Since in reality each transfer step is not impulsive, but has a time spread determined by the transfer time (τ_{hop}), the oscillations will decay due the created phase shifts of the oscillation in the acceptor molecule. To calculate the effect of a nonimpulsive transfer step on the oscillation amplitude, we have to calculate the convolution of the oscillation with the (exponential) transfer function. This problem is analogous to that of the amplitude modulation of signals by a RC low pass filter in electronics. Straightforward calculation yields that in each transfer step the oscillation amplitude is damped with a factor R_s given by

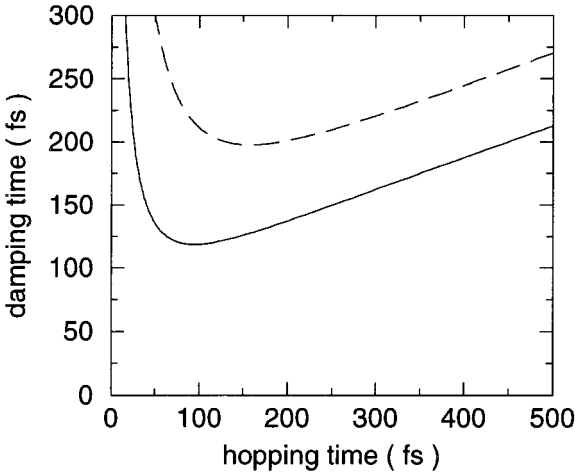

Figure 9. Expected damping time for the 65 (dashed) and 100 cm^{-1} (solid) modes. Curves were calculated using eq 7.

$$R_S = \frac{1}{\left[\left(\frac{2\pi\tau_{hop}}{T_{OSC}}\right)^2 + 1\right]^{1/2}} \tag{5}$$

where R_s is the reduction of the oscillation amplitude per step, τ_{hop} the hopping time, and T_{osc} the period of the oscillation. To relate this reduction per step to the decay time of the oscillation amplitude in case of multiple transfer steps, we use

$$e^{-t/\tau_{damp}} = R_s^{\,t/\tau_{hop}} \tag{6}$$

giving for the decay of the amplitude of the oscillation:

$$\tau_{damp} = \tau_{hop} \ln^{-1}\left[\left(\frac{2\pi\tau_{hop}}{T_{OSC}}\right)^2 + 1\right]^{1/2} \tag{7}$$

For the two oscillatory modes found in *Rps. viridis* (65 and 100 cm^{-1}) the relation between the hopping time and the decay time of the oscillations is given in Figure 9. Since the hopping time is expected to be between 80 and 150 fs, it is clear from the graph that the "hopping"-like model does not apply to explain the long decay times of the oscillations observed in *Rps. viridis* and other bacterial antenna systems. Furthermore, the model describes the decay due to transfer only, which is larger than 1.5 ps (see above). Most essential in the above reasoning is that the transfer step is a pure probability process, or in other words the transfer probability is constant in time. To explain the long damping times found for the oscillations, we have to assume that the transfer rate is a function of the generalized nuclear coordinate, so ($k_{transfer}$(Q)). Actually, as was also noted by others, the oscillations imply that standard theories for excitation transfer do no longer apply.[21,41,62] For instance, one of the assumptions for the Förster transfer theory is that the vibrational relaxation in the donor molecule is much faster than the transfer time between the donor and acceptor. Clearly, the observed vibrations are not in agreement with this constraint. The coherent nuclear motion will cause a modulation of the spectral overlap between the donor and acceptor molecules, and will thereby modulate the probability of transfer between them. A more quantitative theory of transfer between vibrationally excited molecules should be developed to estimate whether such

a theory is capable of explaining the slow decay of the nuclear vibrations in these antenna systems.

V. Concluding Remarks

We summarize that the oscillations seen in *Rps. viridis* are most probably due to vibrations and not due to beating between exciton levels. The size of the oscillations suggests that the Franck−Condon factors are relatively large in this LH-1 antenna compared to Bchl *a* containing systems, which could also be an explanation for the observed fine structure in the low-temperature absorption spectrum. The large oscillations imply that, since the transfer rate between pigments is among others governed by the spectral overlap, the transfer rate is not independent of time. A simple calculation shows that a modification of basic transfer theory is needed to explain the slow decay (∼700 fs) of the oscillations observed. We suggest that a time-dependent transfer rate could play a large role in maintaining the phase relationship between the nuclear motions of donor and acceptor. Even though other (Bchl *a* containing) LH-1 and LH-2 antenna systems show no fine structure in the absorption spectrum, persistent oscillations in these systems have also been observed. An explanation for this could be that inhomogeneous broadening or structural heterogeneity in these systems washes out the bulk spectral features of the vibronic bands. However, also in these systems, the above mechanism could underlie the slow damping of the nuclear oscillations.

Acknowledgment. The authors would like to thank drs. ing. F. Calkoen and Mr. H. A. van der Stroom for the preparation of the *Rps. viridis* membranes and dr. I. H. M. van Stokkum for assistance with the global analysis.

References and Notes

(1) van Grondelle, R.; Dekker, J. P.; Gillbro, T.; Sundström, V. *Biochim. Biophys. Acta* **1994**, *1187*, 1.
(2) Krauss, N.; Schubert, W.; Klukas, O.; Fromme, P.; Witt, H. T.; Saenger, W. *Nature Struct. Biol.* **1996**, *3*, 11, 965.
(3) Rhee, K. H.; Morris, E. P.; Zheleva, D.; Hankamer, B.; Kühlbrandt, W.; Barber, J. *Nature* **1997**, *389*, 522.
(4) Kühlbrandt, W.; Wang, D. N.; Fujiyoshi, Y. *Nature* **1994**, *367*, 614.
(5) Miller, K. R. *Nature* **1982**, *300*, 53.
(6) Stark, W.; Kühlbrandt, W.; Wildhaber, I.; Wehrli, E.; Mühlethaler, K. *EMBO J.* **1984**, *3*, 777.
(7) McDermott, G.; Prince, S. M.; Freer, A. A.; Hawthornthwaite-Lawless, A. M.; Papiz, M. Z.; Cogdell, R. J.; Isaacs, N. W. *Nature* **1995**, *374*, 517.
(8) Zuber, H.; Brunisholz, R. A. In *Chlorophylls*; Scheer, H., Ed.; CRC Press: Boca Raton, FL, 1991; p 627.
(9) Koepke, J.; Xiche, H.; Muenke, C.; Schulten, K.; Michel, H. *Structure* **1996**, *4*, 581.
(10) Karrasch, S.; Bullough, P. A.; Ghosh, R. *EMBO J.* **1995**, *14*, 4, 631.
(11) Fowler, G. J. S.; Visschers, R. W.; Grief, G. G.; van Grondelle, R.; Hunter, C. N. *Nature* **1992**, *355*, 848.
(12) Fowler, G. J. S.; Sockalingum, G. D.; Robert, B.; Hunter, C. N. *Biochem. J.* **1994**, *299*, 3, 695.
(13) Gudowska-Nowak, E.; Newton, M. D.; Fajer, J. *J. Phys. Chem.* **1990**, *94*, 5795.
(14) Koolhaas, M. H. C.; van der Zwan, G.; Frese, R. N.; van Grondelle, R. *J. Phys. Chem. B* **1997**, *101*, 7262.
(15) Monshouwer, R.; Visschers, R. W.; van Mourik, F.; Freiberg, A.; van Grondelle, R. *Biochim. Biophys. Acta* **1995,** *1229*, 373.
(16) McGlynn, P.; Westerhuis, W. H. J.; Jones, M. R.; Hunter, C. N. *J. Biol. Chem.* **1995,** 271, 6, 3285.
(17) Wu, H. M.; Reddy, N. R. S.; Small, G. J. *J. Phys. Chem. B* **1997**, *101*, 651.
(18) Visser, H. M.; Somsen, O. J. G.; van Mourik, F.; van Grondelle, R. *J. Phys Chem.* **1996**, *100*, 18859.
(19) Visser, H. M.; Somsen, O. J. G.; van Mourik, F.; Lin, S.; van Stokkum, I. H. M.; van Grondelle, R. *Biophys. J.* **1995**, *69*, 1083.
(20) Jimenez, R.; Dikshit, S. N.; Bradforth, S. E.; Fleming, G. R. *J. Phys. Chem.* **1996**, *100*, 16, 6825.
(21) Chachisvilis, M.; Pullerits, T.; Jones, M. R.; Hunter, C. N.; Sundström, V. *Chem. Phys. Lett.* **1994**, *224*, 345.
(22) Bradforth, S. E.; Jimenez, R.; van Mourik, F.; van Grondelle, R.; Fleming, G. R. *J. Phys. Chem.* **1995**, *99*, 16179.
(23) Chachisvilis, M.; Sundström, V. *Chem. Phys. Lett.* **1996**, *261*, 165.
(24) Chachisvilis, M.; Fidder, H.; Pullerits, T.; Sundström, V. *J. Raman Spectrosc.* **1995**, *26*, 513.
(25) Nagarajan, V.; Alden, R. G.; Williams, J. C.; Parson, W. W. *Proc. Natl. Acad. Sci. U.S.A.* **1996**, *93*, 13774.
(26) Kennis, J. T. M.; Streltsov, A. M.; Vulto, S. I. E.; Aartsma, T. J.; Nozawa, T.; Amesz, J. *J. Phys. Chem. B* **1997**, *101*, 39, 7827.
(27) Kennis, J. T. M.; Streltsov, A. M.; Permentier, H.; Aartsma, T. J.; Amesz, J. *J. Phys. Chem. B* **1997**, *101*, 41, 8369.
(28) Pullerits, T.; Chachisvilis, M.; Sundström, V. *J. Phys. Chem.* **1996**, *100*, 10787.
(29) Chachisvilis, M.; Kühn, O.; Pullerits, T.; Sundström, V. *J. Phys. Chem. B* **1997**, *101*, 7275.
(30) Hess, S.; Chachisvilis, M.; Timpmann, K.; Jones, M. R.; Fowler, G. J. S.; Hunter, C. N.; Sundström, V. *Proc. Natl. Acad. Sci. U.S.A.* **1995**, *92*, 12333.
(31) Jimenez, R.; van Mourik, F.; Yu, J. Y.; Fleming, G. R. *J. Phys. Chem. B* **1997**, *101*, 7350.
(32) Beekman, L. M. P.; van Mourik, F.; Jones, M. R.; Visser, H. M.; Hunter, C. N.; van Grondelle, R. *Biochemistry* **1994**, *33*, 3143.
(33) Van Mourik, F.; Visschers, R. W.; van Grondelle, R. *Chem. Phys. Lett.* **1992**, *193*, 1.
(34) Reddy, N. R. S.; Small, G. J.; Seibert, M.; Picorel, R. *Chem. Phys. Lett.* **1991**, *181*, 5, 391.
(35) Monshouwer, R.; Abrahamsson, M.; van Mourik, F.; van Grondelle, R. *J. Phys. Chem. B* **1997**, *101*, 37, 7241.
(36) Meier, T.; Chernyak, V.; Mukamel, S. *J. Phys. Chem. B* **1997**, *101*, 37, 7332.
(37) Zhang, F. G.; Gillbro, T.; van Grondelle, R.; Sundström, V. *Biophys. J.* **1992**, *61*, 694.
(38) Greene, B. J.; Farrow, R. C. *Chem. Phys. Lett.* **1983**, *98*, 273.
(39) Wendling, M.; Monshouwer, R.; van Grondelle, R. Manuscript in preparation.
(40) Chachisvilis, M.; Kühn, O.; Pullerits, T.; Sundström, V. *J. Phys. Chem. B* **1997**, *101*, 37, 7275.
(41) Vos, M. H.; Jones, M. R.; Hunter, C. N.; Breton, J.; Lambry, J. C.; Martin, J.-L. *Biochem.* **1994**, *94*, 33, 6750.
(42) Vos, M. H.; Rappaport, F.; Lambry, J. C.; Breton, J.; Martin, J.-L *Nature* **1993**, *363*, 320.
(43) Kleinherenbrink, F. A. M.; Deinum, G.; Otte, S. C. M.; Hoff, A. J.; Amesz, J. *Biochim. Biophys. Acta* **1992**, *1099*, 175.
(44) Cruz, C. H. B.; Gordon, J. P.; Becker, P. C.; Fork, R. L.; Shank, C. V. *IEEE J. Quantum Electron.* **1988**, *24*, 2, 261.
(45) Chachisvilis, M.; Fidder, H.; Sundström, V. *Chem. Phys. Lett.* **1995**, *234*, 141.
(46) Chachisvilis, M.; Sundström, V. *J. Chem. Phys.* **1996**, *104*, 5734.
(47) Visser, H. M. *Thesis, Free University of Amsterdam*, 1996.
(48) Francke, C.; Amesz, J. *Photosynth. Res.* **1995**, *46*, 347.
(49) Visschers, R. W.; Germeroth, L.; Michel, H.; Monshouwer, R.; van Grondelle, R. *Biochim. Biophys. Acta* **1995**, *1230*, 147.
(50) Sauer, K.; Cogdell, R. J.; Prince, S. M.; Freer, A. A.; Isaacs, N. W.; Scheer, H. *Photochem. Photobiol.* **1996**, *64*, 3, 564.
(51) Knox, R. S.; Gülen, D. P*hotochem. Photobiol.* **1993**, *57*, 40.
(52) Kühn, O.; Sundström, V. *J. Chem. Phys.* **1997**, *107*, 4154.
(53) Kühn, O.; Renger, T.; May, V. *Chem. Phys.* **1996**, *104*, 99.
(54) Vos, M. H.; Jones, M. R.; Hunter, C. N.; Breton, J.; Martin, J.-L. *Proc. Natl. Acad. Sci. U.S.A.* **1994**, *91*, 12701.
(55) Rebane, K. K. *Impurity Spectra of Solids*; Plenum Press: New York, 1970.
(56) Cherepy, N. J.; Shreve, A. P.; Moore, L. J.; Boxer, S. G.; Mathies, R. A. *J. Phys. Chem. B* **1997**, *101*, 3250.
(57) Pullerits, T.; Monshouwer, R.; van Mourik, F.; van Grondelle, R. *Chem. Phys.* **1995**, *194*, 395.
(58) Lutz, M. *Biospectroscopy* **1995**, *1*, 313.
(59) Jean, J. M.; Fleming, G. R.; Friesner, R. A. B*er. Bunsen-Ges. Phys. Chem.* **1991**, *95*, 253.
(60) Jean, J. M.; Fleming, G. R. J. *Chem. Phys.* **1995**, *103*, 2092.
(61) Jean, J. M. *J. Chem. Phys.* **1996**, *104*, 5638.
(62) Pullerits, T.; Sundström, V. *Acc. Chem. Res.* **1996**, *29*, 381.